# Statistical and microscopic description of energetic products in the reactions induced by $^{16}O$ on $^{27}Al$, $^{58}Ni$, and $^{197}Au$ at 94 MeV/nucleon

A. Badalá, R. Barbera, and A. Bonasera
*Istituto Nazionale di Fisica Nucleare, Sezione di Catania, Corso Italia 57, I95129 Catania, Italy*

M. Di Toro
*Istituto Nazionale di Fisica Nucleare, Sezione di Catania, Corso Italia 57, I95129 Catania, Italy and Dipartimento di Fisica, Universita' di Catania, Corso Italia 57, I95129 Catania, Italy*

A. Palmeri and G. S. Pappalardo
*Istituto Nazionale di Fisica Nucleare, Sezione di Catania, Corso Italia 57, I95129 Catania, Italy*

F. Riggi and G. Russo
*Istituto Nazionale di Fisica Nucleare, Sezione di Catania, Corso Italia 57, I95129 Catania, Italy and Dipartimento di Fisica, Universita' di Catania, Corso Italia 57, I95129 Catania, Italy*

G. Bizard, D. Durand, and J. L. Laville
*Laboratoire de Physique Corpusculaire, 14032 Caen, France*
(Received 1 August 1990)

Protons and charged pions have been detected at 70°, 90°, and 120° in the reaction induced by $^{16}O$ on various targets at 94 MeV/nucleon incident energy. Measured energy spectra are analyzed in terms of statistical emission from equilibrated sources in a participant-spectator picture. Microscopic dynamical calculations based on the Boltzmann-Nordheim-Vlasov equation are also performed. Experimental data are well reproduced by both models.

## I. INTRODUCTION

Pion production in heavy-ion collisions at energies below the free nucleon-nucleon threshold is still a current problem in nuclear physics at intermediate energies,[1] in spite of a large amount of both inclusive[1,2] and semiexclusive experimental data.[3,4]

Recently, some semiexclusive experiments, in which charged pions have been detected in coincidence with fission fragments[4] and light charged particles,[5] have shown evidence for violent collisions or low impact parameter collisions. However, although a high-energy transfer seems to be at the origin of the emitted pions, the mechanisms which create the pions cannot be easily extracted from the comparison of experimental data and model calculations.

The existing theoretical models cover a large spectrum of very different pictures ranging from the uncorrelated nucleon-nucleon collisions[6] to strongly coherent nucleus-nucleus interactions.[7] Different reaction mechanisms and relative models lead to the same values of inclusive observables such as energy spectra and angular distributions.

Up to now the performed calculations and most part of the experiments have been concerned with neutral pions and charged pions not discriminated in their charge. A more stringent test on the models could be imposed by checking isospin effects through a comparison of the calculations with measured yields of positive and negative pions. Moreover, a systematic comparison of the predictions from two different approaches to the same set of data could point out the most striking features of the involved theoretical descriptions.

A systematic study of the production of charged pions as a function of the target mass has also been previously made with pions detected at 0° only, with a pion energy threshold around 200 MeV/$c$ and a maximum energy near the kinematical limit.[8] The total pion yield is, however, almost entirely exhausted by low-energy pions. By that, we are led to deal with positive and negative pions of kinetic energy less than 100 MeV.

The aim of this work is to discuss only energetic products of the projectile-target collision, such as pions and energetic protons. Low-energy products in their rest frame could generally be attributed to statistical mechanisms. The emission of relatively high-energy protons at large angles, in heavy-ion collisions where a large portion of the incoming linear momentum is distributed in the forward direction, could be considered as a signature of a violent collision and in principle could be associated with a nucleon-nucleon knockout as well as to a preequilibrium emission and/or a statistical emission. The conclusions of Ref. 9 in which high-energy protons, from the reaction $^{27}Al+^{16}O$ at 94 MeV/nucleon, were attributed to a statistical production of a participant zone in a participant-spectator scenario are here reviewed in a context including heavier targets. Pions produced in the same reaction have been attributed to violent collisions or

 

originating from low impact parameter collisions.[5] Then, because of the low impact parameters involved in the collisions producing pions or high-energy protons and the relative smallness of the irradiated target, the spectator nuclear matter (both from target and projectile) is not very large. As a consequence, any interaction of the detected particles with the residual spectator nucleons could be neglected. For massive targets, even for low impact parameter collisions, this residual interaction cannot be neglected so that pion reabsorption and/or rescattering could take place.

Our data are analyzed through two models. The first model is based on the participant-spectator picture in which the emitting source of pions is considered equilibrated in all its degrees of freedom, i.e., spin, isospin, and internal energy distribution. This model has been successfully applied to a semiexclusive pion production study[5] in which pions not discriminated in charge have been detected in coincidence with light charged particles in large area multidetectors. The production of high-energy protons and charged pions is also studied by numerically solving the microscopic Boltzmann-Nordheim-Vlasov (BNV) equation.[10]

The two proposed models contain very different space-time ingredients. The statistical emission of the participant zone in a participant-spectator picture does not take into account the residual interaction of the detected particles with the surroundings nonparticipating nuclear matter, and the emission of particles is obtained at large time scale when the source is very far away from the targetlike and projectilelike fragments. The BNV equation contains essentially the nucleon-nucleon interaction cross section for producing high-energy protons and pions, and the time dependence of the emission of these particles is known. Then the comparison with our data could allow for a better determination of the space-time emission of protons and pions. Moreover, the residual interaction of the emitted nucleons with the others is taken into account. Unfortunately, because of the smallness of the pion production cross section, only perturbative calculations can be performed. Hence the pion reabsorption cannot be properly introduced.

In the present work absolute cross sections for the inclusive spectra of negative and positive pions are presented for several combinations of angles and targets, with an $^{16}O$ beam at 94 MeV/nucleon. In this experiment energetic protons were also identified and their energy spectra were measured at large angles in order to select violent collisions.

## II. EXPERIMENTAL PROCEDURE

In the present experiment a range telescope consisting of ten plastic scintillators ($S_1$–$S_{10}$) and covering a solid angle of 59 msr was used in the detection of charged pions and protons. The telescope was put under vacuum[11] inside the large scattering chamber NAUTILUS at GANIL. It viewed the target from positions between 70° and 120°. In the telescope tuned as a pion detector, the first four scintillators were mainly used for discrimination against the intense proton background. Detectors ($S_5$–$S_9$) are the elements in which stopped pions were detected. The mean pion energy in these elements was 29.3, 40.8, 51.4, 60.9, and 69.8 MeV, respectively. The mean energies of protons stopped in each element, starting from the third one, were 27.4, 43.2, 66.5, 91.2, 113.3, 132.5, and 149.9 MeV. The $S_{10}$ was used as a veto in order to reject all firing particles for which identification was not possible. The background is strongly dependent on the detection angle, due to the forward peaking of fast hydrogen and helium ions, compared to pions in nuclear collisions at these energies ($\simeq 10^4$ particles per emitted pion at forward angles). Thus a powerful hardware rejection of protons is needed to reduce the number of stored events. For pions stopping at $S_i$, the maximum signal at $S_{i-2}$ is always smaller than the minimum signal for protons. A discriminator level set between these two values removed 99% of the background. A complete separation of charged pions from other particles is then obtained by a standard energy-loss analysis. Positive and negative pions were also separated. The method used is that discussed in Ref. 12, based on the decay of the stopped positive pion (with a mean lifetime of 26 ns) producing a monoenergetic muon of 4.2 MeV and a neutrino. This method compares two integrations of the energy pulse, one with a prompt time gate ($Q_p$, "the whole pulse") and the other one with the gate delayed by a $\Delta t \simeq 6$ ns ($Q_d$, "only the tail") with respect to the origin of the signal. The $Q_p$-$Q_d$ correlation is very sensitive to the appearance of the muon signal within the delayed gate, and the relative scatter plot allows for a good separation between the two charge states. The delay $\Delta t$ and the absolute position of the gate against the signal were previously optimized directly irradiating the telescope with very-low-intensity positive- and negative-pion beams. The experimental efficiency was found to be $(80\pm2)\%$ for $\pi^+$ identification. This value is consistent with a $\Delta t \simeq 6$ ns. The negative-pion yield was then deduced by subtracting positive pions from the total pion yield. The numbers of pions produced in the target was obtained after corrections for losses due to the decay in flight and nuclear reactions with the scintillator nuclei ($^{12}C$ and $^1H$). The following interactions were considered: elastic and inelastic scattering and absorption for $^{12}C$, and elastic scattering and radiative capture for $^1H$. Both corrections are energy dependent and were obtained by a Monte Carlo simulation. The overall correction on the detected pion number ranged from 4% at 29 MeV to 40% at 70 MeV pion kinetic energy. Absolute cross sections were obtained by measurement of the beam current with a Faraday cup. The overall uncertainty from beam current and target thickness was around 10%. The corrections for dead time in the data-acquisition system ranged from a few percent at large angles to 10–20 % for the smaller one. The uncertainty in the absolute cross sections was estimated to be around 30% for $\pi^+$ and slightly higher for $\pi^-$.

A different tuning of the associated electronics allowed for the detection of the charged pions or protons. A 1-mm-thick natural lead was placed in front of the telescope in order to absorb soft radiations. The energy loss of the pions and protons in this absorber is taken into ac-

count in the reported energy spectra. The detection angles, for protons, were limited to large values in order to avoid contributions originating from more than one source. Because of this reason, contributions from projectilelike emission are excluded. The exposed targets were $^{27}$Al (6.67 mg/cm$^2$), $^{58}$Ni (8.9 mg/cm$^2$), and $^{197}$Au (19.3 mg/cm$^2$). The target axis was permanently tilted by 60° with respect to the beam direction. A telescope made of three plastic scintillators placed at a fixed angle was used as a monitor. An $^{16}$O beam of $3\times10^9$ particles per second was used.

## III. EXPERIMENTAL RESULTS

The double differential cross section for protons emitted in the reaction induced by a beam of $^{16}$O at 94 MeV/nucleon, on $^{27}$Al, $^{58}$Ni, and $^{197}$Au targets, are reported in Figs. 1(a)–1(c), respectively. The detection angles are, for all measurements, 70°, 90°, and 120°. Error bars indicate statistical fluctuations only. All spectra show an exponential behavior. The slope parameter decreases with the angle, due to kinematical effects related to the velocity of the emitted protons with respect to that of the estimated source. Moreover, the spectra are similar for the different targets.

Figures 2(a)–2(c) report the pion energy spectra, measured at the same angles for the different targets. For unambiguous identification of pions, an energy threshold of 23.9 MeV (corresponding to the mean pion energy in the fifth scintillator of the range telescope) was imposed. Charged pions were separated by using the procedure described in sec. II. All the pion energy spectra show an exponential-like tail toward higher kinetic energies, whereas the characteristic peak near 20 MeV cannot be observed in our case due to the imposed energy threshold. Kinematical effects are in this case less important, so that no strong angle dependence of the spectrum shape is expected for pions. Some deviation from a regular trend can be related to different experimental factors, including proton contamination, especially at the lower energies. Only statistical errors are reported in the figures, while the overall uncertainties in the absolute cross sections are of the order of 30%.

Figures 3(a)–3(c) show the energy spectra for positive and negative pions detected at 90°. A similar result was obtained at 120°, while charge separation is more critical at 70°.

The energy range of the reported pion spectra is too small to extract very reliable values of the slope parameter, since this quantity is usually evaluated by a fit procedure over the energy spectrum over 50 MeV. Anyway, the $\tau=17.1$ MeV value found in Ref. 5 for the reaction $^{16}$O+$^{27}$Al at 94 MeV/nucleon well fits all data at 90° here reported. This value is in agreement with those found for charged pions by Bernard *et al.*[2] for the reaction $^{12}$C+$^{12}$C at comparable incident energies and by Sanouillet *et al.*[2] in the reaction ($^{16}$O,$\pi^{\pm}$) on several target nuclei. Values substantially higher (around 25–30 MeV) have been instead obtained for neutral pions by Noll *et al.*[6] and by Moisan[13] in experiments where lead-glass Cherenkov counters were used to detect the two gamma rays resulting from pion decay. The systematics[1] of the slope parameters deduced from pion energy spectra shows that this quantity changes very little with the bombarding energy below 60 MeV/nucleon, which is not explained by the present models. Also, the discrepancy in the slope parameters deduced from charged- and

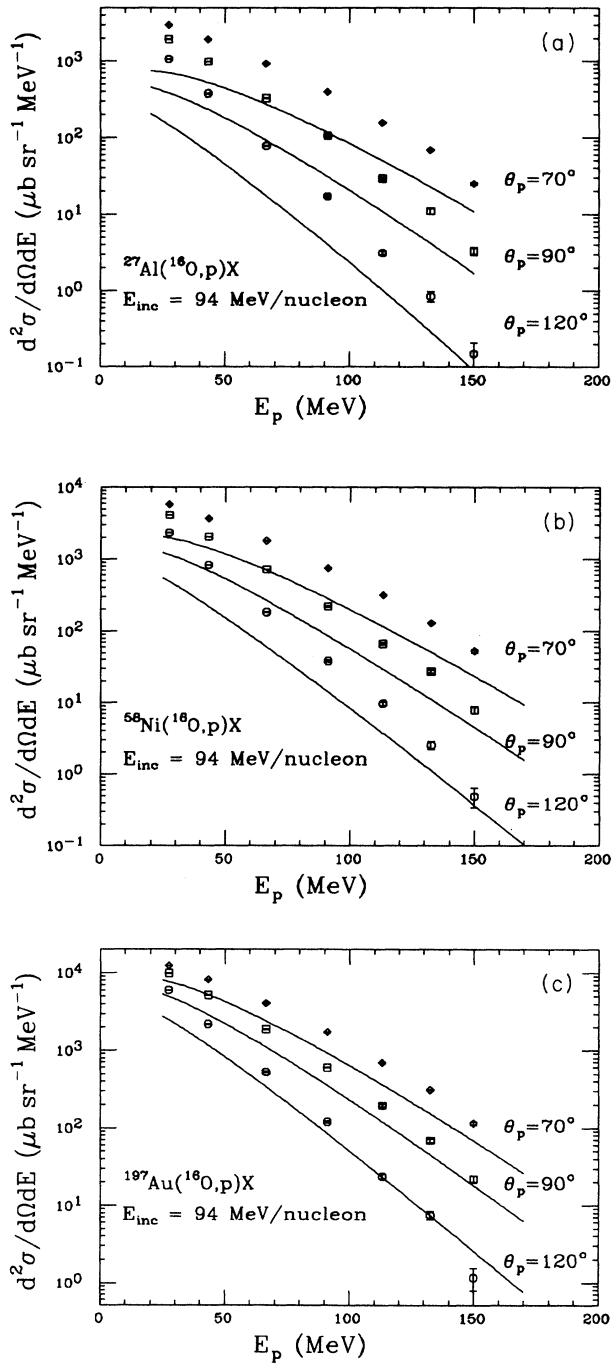


FIG. 1. Proton energy spectra at 70°, 90°, and 120° for (a) $^{16}$O+$^{27}$Al, (b) $^{16}$O+$^{58}$Ni, and (c) $^{16}$O+$^{197}$Au reactions at 94 MeV/nucleon. Solid lines represent the corresponding fireball model calculations (see text).

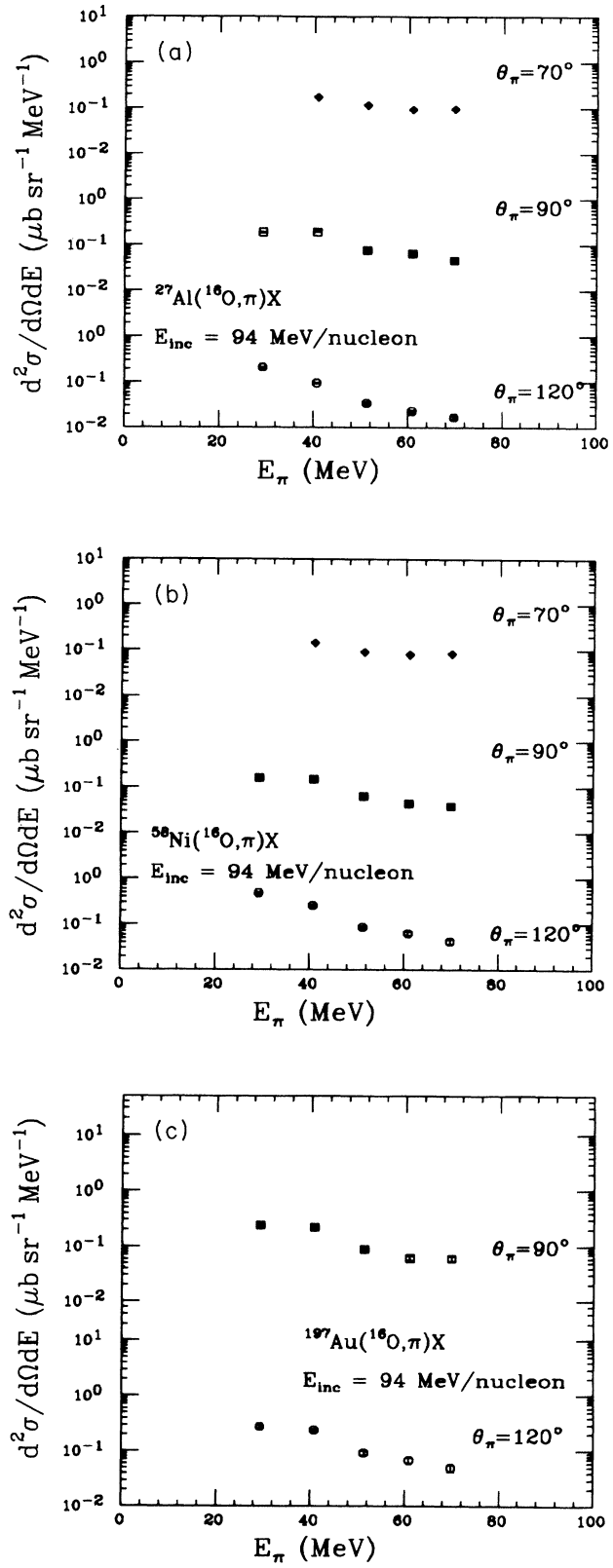


FIG. 2. Pion energy spectra at 70°, 90°, and 120° for (a) $^{16}$O+$^{27}$Al, (b) $^{16}$O+$^{58}$Ni, and (c) $^{16}$O+$^{197}$Au reactions at 94 MeV/nucleon.

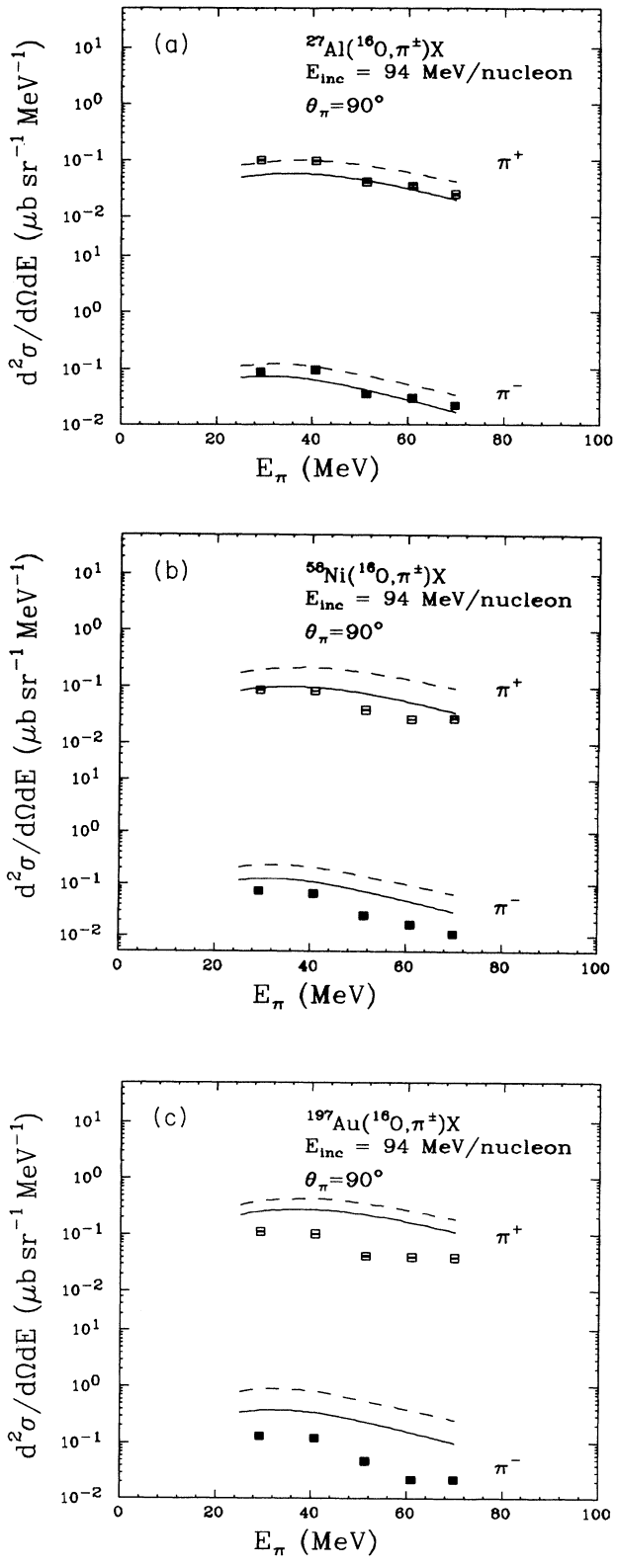


FIG. 3. Energy spectra of positive and negative pions at $\theta$=90° for (a) $^{16}$O+$^{27}$Al, (b) $^{16}$O+$^{58}$Ni, and (c) $^{16}$O+$^{197}$Au reactions at 94 MeV/nucleon. Solid lines represent the predictions of the fireball model calculations. Dashed lines are obtained without the intermediate-energy corrections.

neutral-pion energy spectra at energies around 100 MeV/nucleon need to be further investigated.

## IV. ANALYSIS OF THE DATA WITH A STATISTICAL MODEL

The analysis of the coincidence data reported in Refs. 5 and 9, where the correlation between energetic protons[9] or charged pions[5] with light particles from a $^{27}$Al target was studied, allowed two conclusions to be drawn: (i) The presence of two emission sources of light particles, one source having roughly the velocity of the projectile and the other one a velocity close to that of the center of mass. (ii) The emission of a high-transverse-momentum proton or a pion as a signature of a central collision.

These results suggest a participant-spectator scenario and emphasize the central character of the collision when a high-transverse-momentum proton or a pion is emitted. Consequently, a data analysis in the frame of a participant-spectator model has been performed, with a recently proposed model[14–16] which successfully describes energetic particle production in the energy domain here considered. In such works a standard statistical theory of evaporation is coupled with a modified fireball geometry used to describe the formation of the participant zone.

Many statistical models may be found in the literature. Most of them were constructed for the purpose of describing high-energy nucleus-nucleus collisions (see, for instance, Ref. 17 and references therein). Basically, the reaction is idealized by a two-step process.

(i) A highly excited zone is created, the so-called "fireball." Its size is governed mainly by geometrical considerations.[18] The energetics of such a highly excited zone is very often calculated neglecting fast emission processes (PEP's) and energy dissipation via collective modes.

Concerning the energetics of the fireball, the model used here takes into account both preequilibrium emissions and dissipation via collective modes. These effects, together with the Pauli blocking, modify the size and energetics of the fireball: The number of participant nucleons is reduced with respect to the geometrical abrasion value,[8] and the energetics of the fireball is affected since some energy is dissipated in the spectators through a nucleon-exchange mechanism.

These assumptions are relevant at energies below 100 MeV/nucleon. However, at 94 MeV/nucleon and with a beam of $^{16}$O, the authors of Ref. 9 have shown that these intermediate-energy corrections are not so important for a light target. Here we show that, for heavier target nuclei, these corrections are not negligible. As an example, the nucleon number ($A_{\rm fire}$) and the excitation energy per nucleon ($E^*$) of the fireball is shown in Fig. 4, for the Al, Ni, and Au targets. For the Al target the slight difference in the two distributions of the nucleon number $A_{\rm fire}$, for the fireball model calculations with (solid line) and without (dashed line) intermediate-energy corrections, is washed out by the impact parameter integration. A large difference due to the intermediate-energy corrections is instead observed in the case of the $^{197}$Au target. At $b=1$ fm, without the intermediate-energy corrections, $A_{\rm fire}$ assumes increasing values: 34, 48, and 64 for Al, Ni, and Au, respectively. Introducing these corrections, a saturation effect of $A_{\rm fire}$ as a function of the target mass can be observed.

(ii) The decay of the hot zone is considered. This decay is described by the Weisskopf theory.[9] In Refs. 14–16 the Weisskopf theory has been used to calculate subthreshold pion and high-energy gamma-ray production rates in rather good agreement with the data. In the description of the decay process, we only consider the emission of seven kinds of particles: neutrons, protons, deuterons, tritons, $^3$He, alpha particles, and pions of both charges. We assume that heavier particle emission can be

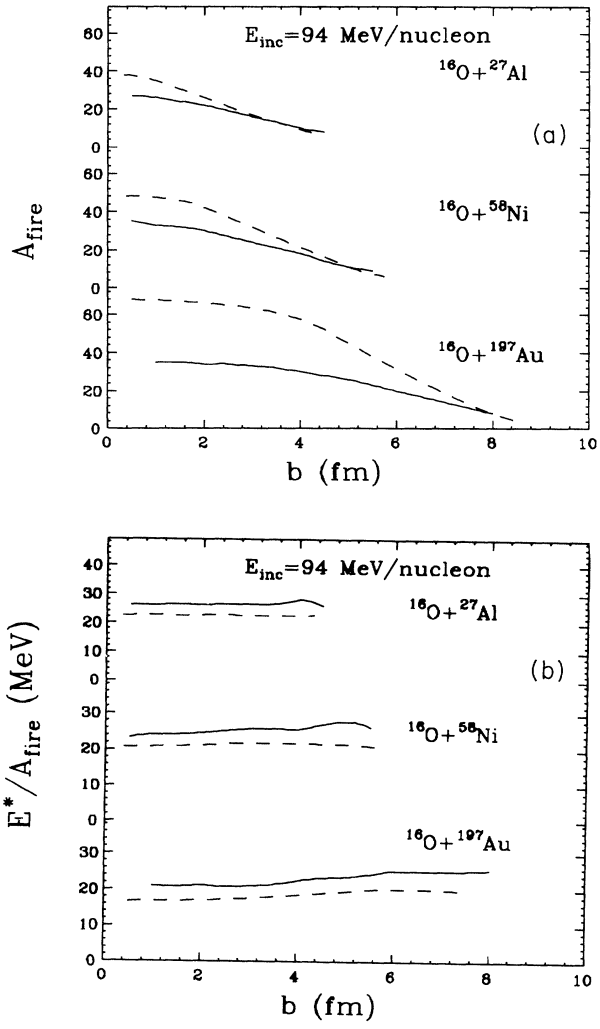


FIG. 4. (a) Number of nucleons of the fireball formed in the reaction induced by $^{16}$O at 94 MeV/nucleon on $^{27}$Al, $^{58}$Ni, and $^{197}$Au targets as a function of the impact parameter. Dashed and solid lines refer to the predictions of the fireball model without and with intermediate-energy corrections, respectively. (b) Excitation energy per nucleon of the fireball for the same systems as in (a) as a function of the impact parameter. Dashed and solid lines refer to the predictions of the fireball model without and with intermediate-energy corrections, respectively.

neglected in agreement with the assumption of Ref. 20.

We briefly recall the Weisskopf theory and the derivation of the inclusive cross section for a given particle $j$. Let us consider the following process at step $s$:

$$A^* \rightarrow (A-j)+j \ .$$

The transition rates are

$$w(s,p_j)=g_j \frac{p_j}{E_j} \frac{\sigma_{\text{inv}}(s)}{(2\pi\hbar)^3} \frac{\rho(E(s))}{\rho(E^*(s))} \ , \tag{1}$$

where $p_j$, $E_j$, and $g_j$ stand for the momentum, total energy, and degeneracy factor of particle $j$, $\sigma_{\text{inv}}$ is the cross section for the inverse process, and $E^*(s)$ and $E(s)$ are the excitation energies of the fireball before and after the evaporation of the particle $j$, respectively. Since we deal with light particles, $\sigma_{\text{inv}}$ is taken in the geometrical limit, although we take into account the Coulomb barrier. For the pion production the inverse absorption cross section is obtained from the parametrization of Ref. 21, which is valid in the energy range 37–280 MeV. In order to obtain the inverse cross sections in our pion energy range, we linearly extrapolated this parametrization down to 25 MeV. The density of states of the initial and final nuclei are calculated within the Fermi gas model using the parametrization of Ref. 20. The emission probability at step $s$ of a particle $j$ with respect to the other particles is

$$W_s(j)=\frac{w(s,p_j)}{\sum_i \int w(s,p_i)d^3p_i} \ . \tag{2}$$

Thus the invariant cross section is

$$E_j^{\text{lab}} \frac{d^3\sigma}{d^3p_j^{\text{lab}}}=2\pi \int b \sum_s E_{\text{c.m.}}(s) W_s(j) db \ , \tag{3}$$

where $E_{\text{c.m.}}(s)$ is the total energy of the particle $j$ in the c.m. of the fireball at impact parameter $b$, and step $s$ corresponds to a given $p_{\text{lab}}$ and $E_{\text{lab}}$. The sum runs over all the possible steps of the decay process. The process is stopped when the system is stable against particle emission or reduced to a light particle ($A=4$).

We performed a complete simulation of the decay process by means of a Monte Carlo method. To do this, at each step of the process the particle width for the emission of each type of particle is evaluated. A particle is then chosen and its velocity randomly selected from a thermalized distribution according to the temperature of the system at the step under consideration. The emission of the detected particle is considered at each step, thus counting correctly the first, second, . . . , $n$th chance of emission. Momentum and energy conservation are correctly treated at each step of the decay. The emission of charged particles is properly treated by inclusion of the Coulomb barrier.

It should be noted that one of the major drawbacks of the model is that it only takes into account particles emitted by the fireball, so that particles coming from the quasitarget and from the quasiprojectile are not accounted for. We observe that detection angles are here very large. This excludes contributions from projectilelike fragments. On the other hand, the energy of the detected particles is large enough, and their emission from the excited targetlike fragments can be excluded at least for the $^{27}$Al target. For heavier targets some contribution to the proton spectra, from the targetlike fragments, could affect only the low-energy components.

In Figs. 1(a)–1(c) experimental and calculated spectra of protons emitted at 70°, 90°, and 120° are shown for the Al, Ni, and Au targets, respectively. Solid lines are the result of the statistical model calculations. The agreement between the data and the calculation is not very good, especially in the low-energy domain where the experimental yield is underestimated. The calculated spectra are too flat, indicating that too much energy has been put into the system. This might be due to the fact that the emission of preequilibrium particles by the fireball is not included, thus leading to an overestimate of the excitation energy of the system. A better agreement is obtained going from a low-mass target toward the heavier one. For the Au target both absolute yields and slopes of the energetic spectra are quite well reproduced at all angles. This is probably due to the fact that the statistical model works better with more involved nucleons.

Figures 3(a)–3(c) show experimental and calculated energy spectra of positive and negative pions detected at 90° for the three targets. Solid lines are referred to the present model calculations, while dashed curves are obtained without the intermediate-energy corrections. No fitting parameter was used. It is evident that both positive- and negative-pion yields are well reproduced. This is due, on the one hand, to the satisfactory parametrization of the inverse absorption cross section and, on the other hand, to the reasonable ratio of the number of protons and neutrons in the fireball.

However, while the agreement is fairly good for the $^{27}$Al target, for both charged-pion yields the calculations overestimate the experimental cross section for the heavier systems. A possible explanation of this increasing disagreement with the target mass could be due to the reabsorption of the pion in the surrounding nuclear matter. This reabsorption should increase with the mass of the target because of the mean free path of the pion in nuclear matter ($\lambda_\pi \simeq 3$ fm in the energy range of the observed pions).

## V. BOLTZMANN-NORDHEIM-VLASOV CALCULATIONS

A dynamical calculation of the collision process was performed by the BNV equation, with the aim of studying the emission of energetic protons and pions.

The BNV equation was numerically solved by means of the test particle method,[10], i.e., expressing the phase space as a collection of $N(A_1+A_2)$ test particles. $A_1$ and $A_2$ are the mass numbers of the colliding nuclei, and $N$ is the number of test particles per nucleon. The time evolution of the test particles was followed through the Hamiltonian equation of motion with a Skyrme mean field, giving $K=200$ MeV compressibility. Momentum changes of the test particles were allowed during the time evolution due to individual N-N collisions. The collision integral of the BNV equation was simulated by the mean

free path.[22,23]

Each test particle was represented by a Gaussian to get a smooth distribution function in the phase space. At the starting time the test particles are randomly chosen in two shifted Fermi spheres in momentum space. The initial available momentum distributions are an essential ingredient of the calculation, since it is known[24] that different configurations can give photon spectra which differ in magnitude by a factor of 3–4 in the region around the pion rest mass. To check whether this approach could give a reasonable description of heavy-ion collisions at these energies, proton inclusive yields were first calculated. Nucleon emission was allowed for in the simulation by comparison of the kinetic energy of the involved particles and the Coulomb barrier, and then checking for the presence of other particles in the surroundings. Figures 5(a)–5(c) report different energy spectra, for the $^{16}O+^{27}Al$ and $^{16}O+^{58}Ni$ cases. The proton yield was obtained from the final phase-space distribution, by integration over the impact parameter $b$, with step $\Delta b = 1$ fm. Between 100 and 150 test particles per nucleon were employed in the present calculations.

As can be seen from Fig. 5, the agreement both in shape and absolute magnitude is very good up to energies around 150 MeV, even though the values of the calculated cross sections at the higher energies are affected by large statistical errors (about 40% against 5–10 % at low energies). Calculations were performed with the same sets of parameters, whatever the detection angle and target mass are. This allows one to be confident in the phase-space description, from which to estimate the pion yield.

It is known that subthreshold pion production is characterized by a low cross section as compared to the proton yield. For this reason the pion yield was evaluated by a perturbative approach.[23] Each individual nucleon-nucleon collision gives a contribution to the cross section for pion production through its probability of producing a pion with a given kinetic energy and emission angle. This gives better statistics for the events of interest, which would be otherwise unattainable in the conventional approach. The elementary cross sections for pion production were taken from the parametrization of Ver West and Arndt.[25]

Pion energy spectra have been seldom calculated in the BNV approach.[1] A few reported cases[26–28] show theoretical spectra harder than the experimental ones. Figure 6 shows the result of our calculations compared to the experimental spectra for the $^{16}O+^{27}Al$ reaction at 70°, 90°, and 120°. The dashed line is the result of the calculation. As can be seen, the theory overestimates the experimental cross section at 90° and 120°, but the shape is well reproduced. At 70° the agreement is not so good, since the experimental spectrum is rather flat for energies larger than 50 MeV [see Fig. 6(a)].

It is known that neglecting the pion reabsorption ($\lambda_\pi = \infty$), the calculations overestimate the experimental spectra. Pion reabsorption is frequently taken into account in a semiempirical way, introducing an attenuation factor $P = \exp(-R/\lambda_\pi)$, where $R$ is the average path which a pion has to traverse to escape from the nuclear matter and $\lambda_\pi$ denotes the average pion mean free path. Mean free paths ranging from 3 to 6 fm have been used in the past to reproduce absolute cross sections. Theoretical calculations have been also performed[29,30] to evaluate the energy dependence of $\lambda_\pi$ according to different assumptions.

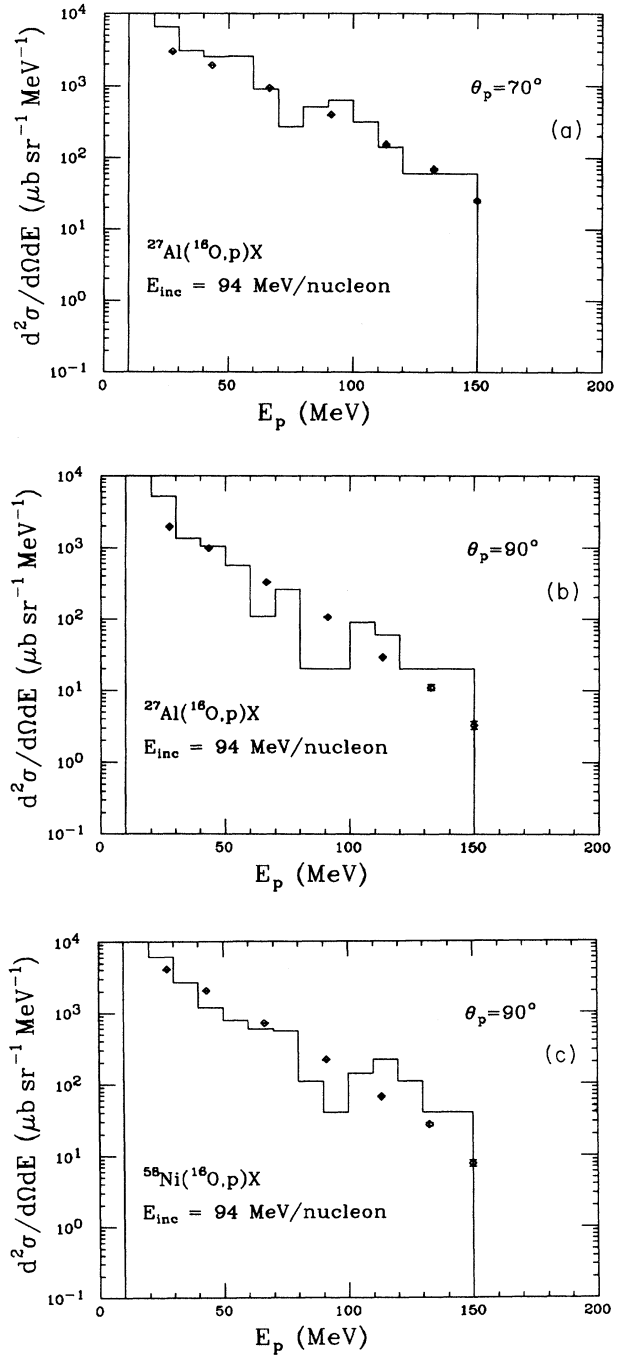


FIG. 5. Comparison between experimental proton energy spectra and the result of a microscopic calculation based on the Boltzmann-Nordheim-Vlasov equation. (a) $^{16}O+^{27}Al$ at 70°, (b) $^{16}O+^{27}Al$ at 90°, and (c) $^{16}O+^{58}Ni$ at 90°.

It has been suggested[13] that data taken on different targets could help to extract useful information about the energy dependence of the pion mean free path. If the primary invariant cross section is assumed to be dependent only on the target mass, then one can use the ratios of pion energy spectra or angular distributions measured for different targets to investigate the reabsorption effects.

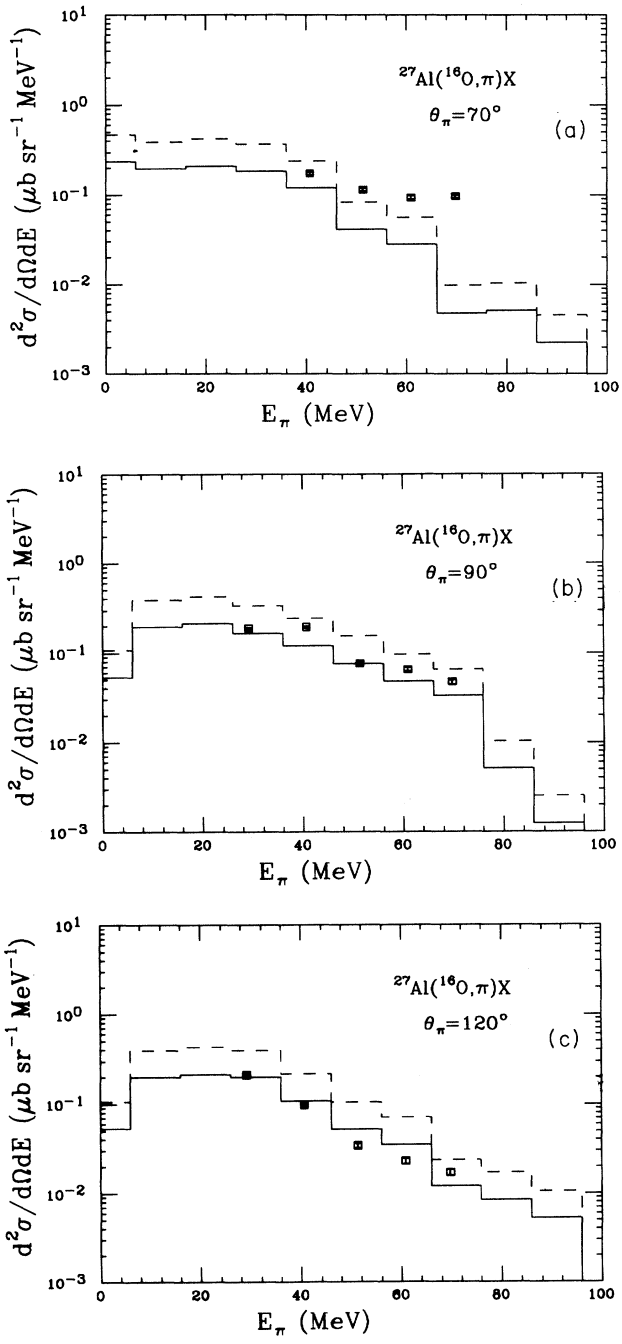


FIG. 6. Pion energy spectra as compared to the result of a microscopic calculation based on the Boltzmann-Nordheim-Vlasov equation (dashed lines). Solid lines are obtained with a pion reabsorption factor (see text). (a) $^{16}$O+$^{27}$Al at 70°, (b) $^{16}$O+$^{27}$Al at 90°, and (c) $^{16}$O+$^{27}$Al at 120°.

Along this line, the pion survival probability, as a function of the pion kinetic energy, is given by

$$P(A_1, A_2, T_\pi) = \frac{[(1/\sigma)(d\sigma/dT)]_{A_1}}{[(1/\sigma)(d\sigma/dT)]_{A_2}}, \quad (4)$$

where each energy spectrum is normalized to the integrated cross section $\sigma$, with $A_1$ greater than $A_2$.

Figure 7 reports the ratios $P(A_1, A_2, T_\pi)$ extracted by a comparison of the experimental cross sections for $\pi^+$ and $\pi^-$ at $\theta$=90° from the reactions on $^{27}$Al, $^{58}$Ni, and $^{197}$Au. Because the total cross sections are not available, the reported $P$ ratios give only the relative energy dependence of the reabsorption probability. The comparison was made in the laboratory system. For forward and backward angles kinematical effects must be taken into account allowing the pion emission from different targets in their respective average source rest frame. No clear energy dependence of the reabsorption effects is seen from these data, at variance with the findings of Refs. 29 and 30. For this reason it was decided to use a constant mean free path in estimating the pion reabsorption effects. A best fit to the data for the $^{16}$O+$^{27}$Al reaction at $\theta$=120° gives a value of $\lambda$ of around 6 fm. This value was used to scale the calculations also for the other angles. The average distance traversed by the pion was estimated by the parametrization reported by Cassing.[31] Calculated pion spectra with the above-mentioned procedure are reported in Fig. 6 as solid lines.

Figure 8 shows the result of a similar calculation for the $^{197}$Au target. The required mean free path to fit the energy spectrum at $\theta$=120° was found to be larger ($\lambda_\pi$=7.5 fm) for the $^{197}$Au case.

Isospin effects were also checked by a comparison of the $\pi^+$ and $\pi^-$ yields with the corresponding prediction of the BNV calculations. Figure 9 shows the result for the $^{27}$Al target at $\theta$=90°. Dashed and solid lines refer, as before, to the predictions of the model without and with pion reabsorption, respectively.

A large difference (in some cases by a factor of 3) in the calculated cross sections for $\pi^+$ and $\pi^-$ is found, at variance with experimental data. This cannot be explained by the uncertainties associated to the pion charge separation procedure, since these are of the order of 30%. This effect could come from some imperfection in the descrip-

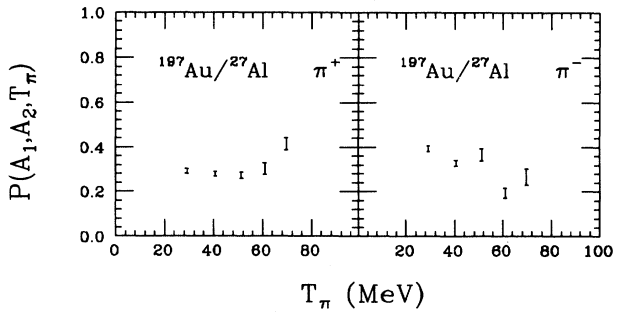


FIG. 7. The pion survival probability, as obtained from the ratio of energy spectra on different targets (see text).

tion of the initial proton and neutron phase-space distribution of the colliding nuclei, since the $\pi^+/\pi^-$ ratio is mainly governed by the elementary cross section and the relative distribution of protons and neutrons in the interacting nuclei. However, the same microscopic approach is able to reproduce[23] the ratio of $\pi^+$ to $\pi^-$ for large pion kinetic energies in the La+La case at 246 MeV/nucleon.

To further investigate the mechanism of pion emission, it is important to know the time and space distribution of the emitting source. The average primary collision time was found to vary[32] smoothly with the bombarding energy; it is expected to be around 10 fm/$c$ at the energy employed in the present investigation.

Pions as well as high-energy photons are expected to be produced in the early stage of the heavy-ion collision. This is due to the fact that when nucleon-nucleon collisions occur, starting to fill the phase space, the availability of final-state phase-space channels in the latter stages of the process is greatly reduced. Moreover, the production rate of energetic particles and photons is influenced by the high components of the momentum distribution, which are greatly reduced by nucleon-nucleon collisions.

Figure 10 shows the time distribution of the contribu-

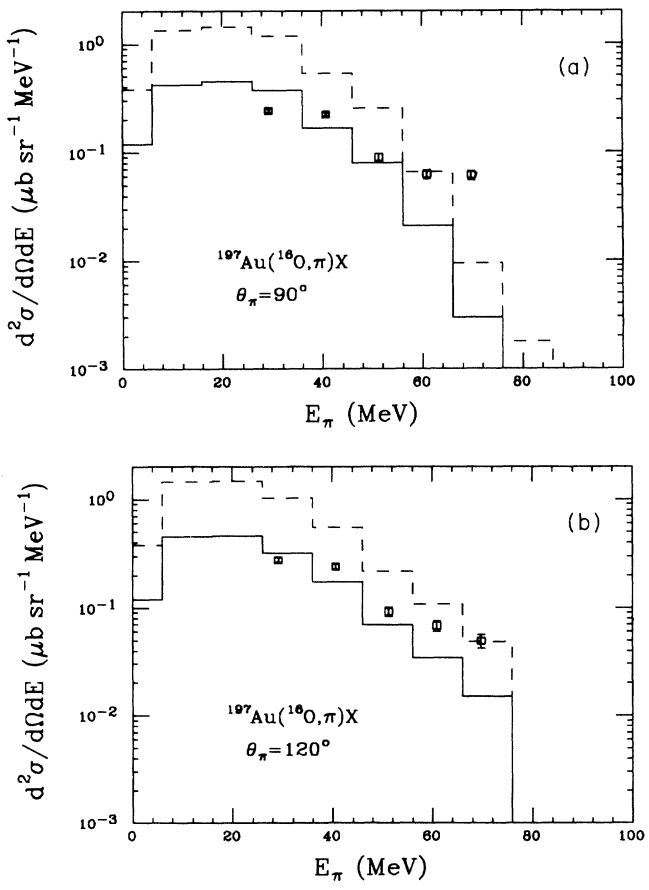


FIG. 8. Same as Fig. 6, for the $^{16}$O+$^{197}$Au reaction at 94 MeV/nucleon at (a) 90° and (b) 120°.

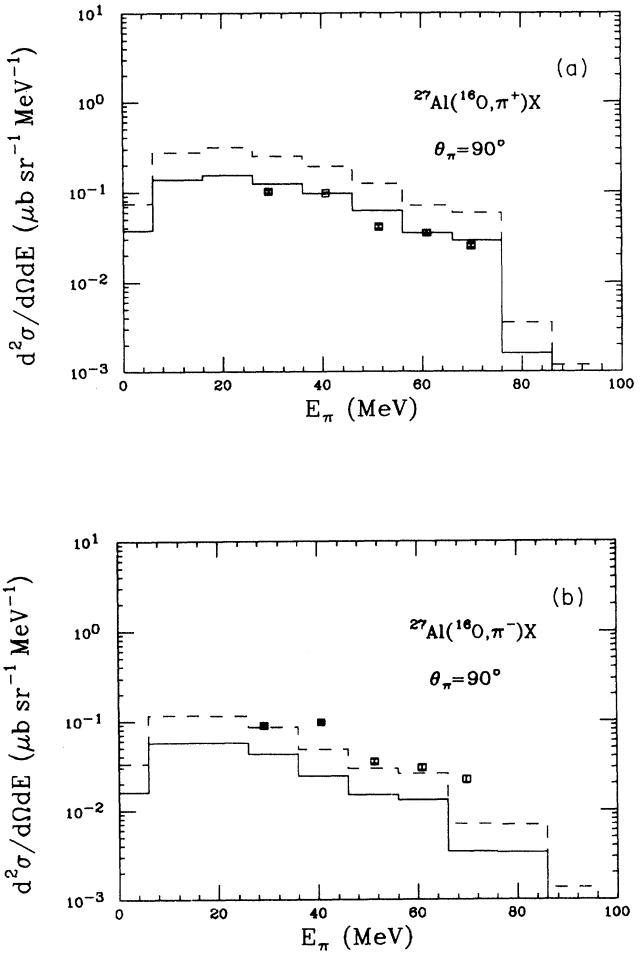


FIG. 9. Charged-pion energy spectra at $\theta$=90°, for the $^{16}$O+$^{197}$Au reaction. Dashed and solid lines show the result of the microscopic calculation without and with pion reabsorption effects. (a) Positive pions and (b) negative pions.

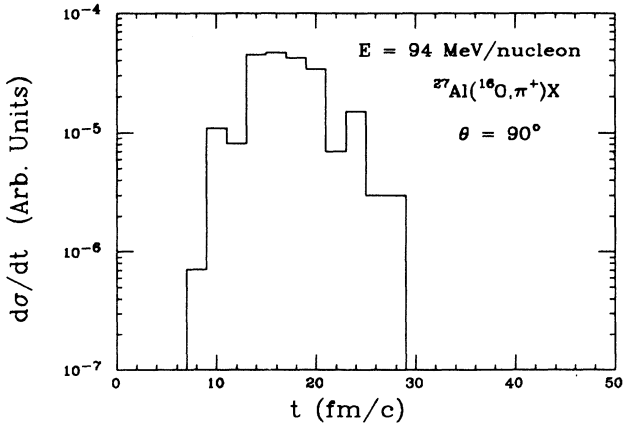


FIG. 10. Time evolution of the positive-pion production rate at 90° in the BNV approach for the reaction $^{16}$O+$^{27}$Al at 94 MeV/nucleon.

tion to the $\pi^+$ production for the $^{16}O+^{27}Al$ reaction, as estimated by the model. It is seen that most of the pion production comes from collisions occurring within 25–30 fm/$c$. Similar results are also obtained for the other cases.

## VI. CONCLUSIONS

The inclusive yield of energetic products, as high-energy protons and charged pions, has been investigated with an $^{16}O$ beam at 94 MeV/nucleon on three targets, spanning a wide range of masses. These products are believed to give similar information if they come from the same source. It has been already shown[5,9] that the multiplicity of charged particles going to forward angles is nearly the same when triggered by 150-MeV protons or by a pion of equivalent total energy. Also, the velocity spectra of light charged particles emitted at forward angles in coincidence with pions or high-energy protons are very similar. These data suggest that these two probes select the same space-time distribution of the residual nuclear matter.

A comparison of inclusive data was then made with the predictions from two different models. In the statistical approach the space-time evolution of the nuclear matter requires large times, and only a portion of the colliding nuclei defines the energetics of the emitting source with no interaction with the spectators. On the other hand, in the dynamical calculations based on the nucleon-nucleon collisions the space-time evolution of all nucleons is described, and the time at which the production of the particles occurs can be expressly extracted.

Both models were seen to give a reasonable agreement with the data, despite the large difference in the involved time scale.

The statistical model, where a modified fireball geometry was introducing taking into account intermediate-energy corrections, although able to reproduce the gross features of exclusive data[5] such as correlations between pions and light charged particles, systematically underestimates the inclusive proton yield. The model predicts also energy spectra which are flatter than the experimental ones. This could be due to an overestimation of the excitation energy per nucleon of the fireball; this in turn is to be related to the lack of preequilibrium particle emission from the fireball. The positive- and negative-pion energy spectra are well reproduced by the statistical model calculations in the case of the $^{27}Al$ target. For the heavier targets the ratio of $\pi^+/\pi^-$ is still well predicted, thus showing that the calculated number of protons and neutrons is properly evaluated. With an increase of the mass of the target, the theoretical calculations overestimate the pion yield (by a factor of 2–3 for the $^{197}Au$ target). This could be related to reabsorption effects (which increase with the increasing target mass), which are not properly included in the model, since this does not take into account all the nuclear matter belonging to projectile and target.

The comparison of the proton spectra for all targets and angles to the predictions of the microscopic calculations gives a quite good agreement, both for the slope and the absolute values of the cross sections. Contrary to what happens in the statistical model, this microscopic calculation accounts for all nucleons in the projectile and target, and takes into account in a natural way the possible preequilibrium emission. This could be at the origin of the good agreement for the absolute yield and slope of the proton energy spectra. The main aspects of the microscopic calculations lead also to a good agreement with the pion energy spectra. The slight overestimation of the absolute cross sections is probably due to the reabsorption effects which have to be included through the usual semiempirical procedure. This results in values of the mean free path of around 6–7 fm, which is larger than the values extracted from experiments on pion absorption on nuclei (about 3 fm at these pion energies). It can be observed, however, that the parametrization proposed in Ref. 31 for the mean distance traversed by the pions also influences the obtained values of $\lambda_\pi$. Moreover, the nucleon-nucleon collisions which are described in the microscopic calculations dynamically modify the normal density of the nuclear matter, so that the reported values of $\lambda_\pi$ could not be directly compared to those extracted from pion absorption experiments.

In conclusion, an overall better agreement with the experimental data is obtained through the microscopic description of the interacting nuclear matter. It should be observed that the evolution of the nuclear matter by a dynamical calculation can in principle result in an equilibrated source, which could be described also in the statistical model approach.

Of course, only a selected part of the phase space is probed by the data reported here. For this reason it could be interesting to test the capability of a dynamical approach also to exclusive experiments. Unfortunately, it is not so easy to account for the emission of complex particles or to calculate many-body observables such as multiplicities and angular distributions of the particles associated with the production of a high-energy probe. This is due to the lack of two- or more-body correlations in such kinetic theories which are based at the one-body level. Recent attempts to account for the production of complex particles have been reported.[33,34]

We wish to thank C. D'Amato, F. Librizzi, D. Nicotra, and C. Rapicavoli for their technical support before and during the run.

[1]P. Braun-Munzinger, in *Proceedings of the 1989 International Nuclear Physics Conference, Sao Paulo, Brazil* (World Scientific, Singapore, 1989), p. 641, and references therein; W. Benenson, Nucl. Phys. **A482**, 503c (1988).

[2]E. Grosse, Nucl. Phys. **A447**, 611c (1986); V. Bernard *et al.*, *ibid.* **A423**, 511 (1984); G. Sanouillet *et al.*, Nuovo Cimento A **99**, 875 (1988).

[3]S. Aiello *et al.*, Europhys. Lett. **6**, 25 (1988).

[4]B. Erasmus *et al.*, Nucl. Phys. **A481**, 821 (1988).

[5]R. Barbera *et al.*, Nucl. Phys. A (to be published).

[6]H. Noll *et al.*, Phys. Lett. **52**, 1284 (1984).
[7]J. Stachel *et al.*, Phys. Rev. C **33**, 1420 (1986).
[8]E. Chiavassa *et al.*, Nucl. Phys. **A422**, 621 (1984).
[9]D. Durand *et al.*, Nucl. Phys. **A511**, 442 (1990).
[10]G. Bertsch and S. Das Gupta, Phys. Rep. **160**, 190 (1988), and references therein.
[11]D. Nicotra, F. Librizzi, and C. Rapicavoli, Internal Report No. INFN/TC-88/20, 1988 (unpublished).
[12]J. Julien, in Proceedings of the 3rd International Conference on Nuclear Reaction Mechanisms, Varenna, Italy, 1983 (unpublished), p. 599; see also Ref. 2.
[13]C. Moisan, Master of Science thesis, McGill University, 1990 (unpublished).
[14]A. Adorno, A. Bonasera, M. Di Toro, C. Gregoire, and F. Gulminelli, Nucl. Phys. **A488**, 451c (1988).
[15]A. Bonasera, M. Di Toro, and C. Gregoire, Nucl. Phys. **A483**, 738 (1988); M. Prakash, P. Braun-Munzinger, J. Stachel, and N. Alamanos, Phys. Rev. C **37**, 1959 (1988).
[16]A. Bonasera, M. Di Toro, and C. Gregoire, Nucl. Phys. **A463**, 563 (1987).
[17]S. Das Gupta and A. Z. Mekjian, Phys. Rep. **72**, 132 (1981).
[18]J. Gosset, H. H. Gutbrod, W. G. Meyer, A. M. Poskanzer, A. Sandoval, R. Stock, and G. D. Westfall, Phys. Rev. C **16**, 629 (1977).
[19]V. Weisskopf, Phys. Rev. **52**, 295 (1937).
[20]J. Aichelin and G. Bertsch, Phys. Lett. **164B**, 350 (1984).
[21]A. Bonasera and G. Bertsch, Phys. Lett. B **195**, 521 (1987).
[22]A. Bonasera, G. F. Burgio, and M. Di Toro, Phys. Lett. B **221**, 233 (1989).
[23]A. Bonasera, G. Russo, and H. H. Wolter, Phys. Lett. B **246**, 337 (1990).
[24]K. Niita, W. Cassing, and U. Mosel, Nucl. Phys. **A504**, 391 (1989).
[25]B. J. Ver West and R. A. Arndt, Phys. Rev. C **25**, 1979 (1982).
[26]M. Blann, Phys. Rev. Lett. **54**, 2215 (1985).
[27]M. Blann, Phys. Rev. C **32**, 2215 (1985).
[28]W. Bauer, Phys. Rev. C **40**, 715 (1989).
[29]J. Hufner and M. Thies, Phys. Rev. C **20**, 273 (1979).
[30]R. A. Mehren, H. M. Radii, and J. O. Rasmussen, Phys. Rev. C **30**, 301 (1984).
[31]W. Cassing, Z. Phys. A **329**, 487 (1988).
[32]W. Cassing, Z. Phys. A **327**, 447 (1987).
[33]J. Aichelin, G. Peilert, A. Bohnet, A. Rosenhauer, H. Stocker, and W. Greiner, Nucl. Phys. **A488**, 437c (1988).
[34]A. Bonasera and F. Gulminelli, Phys. Lett. B (submitted).